

# GTA: Grouped-head latenT Attention

**Luoyang Sun**<sup>1,2,3</sup>, **Cheng Deng**<sup>3,4,\*</sup>, **Jiwen Jiang**<sup>1,2,3</sup>, **Xinjian Wu**<sup>5</sup>,  
**Haifeng Zhang**<sup>1,2,\*</sup>, **Lei Chen**<sup>4,6</sup>, **Lionel M. Ni**<sup>4</sup>, **Jun Wang**<sup>5,7,\*</sup>

<sup>1</sup>Institution of Automation, Chinese Academy of Sciences

<sup>2</sup>School of Artificial Intelligence, University of Chinese Academy of Sciences

<sup>3</sup>AI Lab, The Yangtze River Delta

<sup>4</sup>The Hong Kong University of Science and Technology (Guangzhou)

<sup>5</sup>University College London

<sup>6</sup>The Hong Kong University of Science and Technology

<sup>7</sup>UCL Centre for Artificial Intelligence

davendw49@gmail.com, haifeng.zhang@ia.ac.cn, jun.wang@cs.ucl.ac.uk

## Abstract

Attention mechanisms underpin the success of large language models (LLMs), yet their substantial computational and memory overhead poses challenges for optimizing efficiency and performance. A critical bottleneck arises as KV cache and attention computations scale rapidly with text length, challenging deployment on hardware with limited computational and memory resources. We observe that attention mechanisms exhibit substantial redundancy, since the KV cache can be significantly compressed and attention maps across heads display high similarity, revealing that much of the computation and storage is unnecessary. Leveraging these insights, we propose **GrouPed-Head LatenT Attention (GTA)**, a novel attention mechanism that reduces memory usage and computational complexity while maintaining performance. GTA comprises two components: (1) a shared attention map mechanism that reuses attention scores across multiple heads, decreasing the key cache size; and (2) a nonlinear value decoder with learned projections that compresses the value cache into a latent space, further cutting memory needs. GTA cuts attention computation FLOPs by up to 62.5% versus Grouped-Query Attention and shrink the KV cache by up to 70%, all while avoiding the extra overhead of Multi-Head Latent Attention to improve LLM deployment efficiency. Consequently, GTA models achieve a 2 $\times$  increase in end-to-end inference speed, with prefill benefiting from reduced computational cost and decoding benefiting from the smaller cache footprint. [Project website](#)

## 1 Introduction

Large language models (LLMs) have revolutionized natural language processing, driving breakthroughs in text generation, reasoning, and contextual understanding [1, 2]. The attention mechanism, a core component of these models, enables selective focus on relevant parts of the input sequence, underpinning their expressive power [3]. However, the memory and computational demands of attention, particularly the key-value (KV) cache in autoregressive generation, pose significant challenges for long-context scenarios and resource-constrained environments [4, 5]. These bottlenecks limit the scalability of LLMs in practical applications, where memory efficiency and low-latency inference are critical.

\*Correspondence to [Cheng Deng](#), [Haifeng Zhang](#), [Jun Wang](#).

Prior efforts to mitigate attention-related challenges in large language models (LLMs) have led to several innovations. Multi-Head Attention (MHA) [3], the foundation of modern transformers, projects input sequences into multiple query, key, and value representations to capture diverse contextual patterns, but its KV cache scales poorly with sequence length, limiting long-context applicability. Multi-Query Attention (MQA) [6] reduces memory usage by sharing a single key-value pair across heads, yet sacrifices expressivity. Grouped-Query Attention (GQA) [7] groups heads to balance efficiency and performance, but compromises attention granularity. Multi-head Latent Attention (MLA) [8] compresses the KV cache while preserving representational capacity, but its high computational overhead restricts use in resource-constrained settings. Other methods, such as differential attention [9] and convolution-augmented attention [10], improve contextual focus, but often increase complexity. These approaches are limited by high computational overhead, inefficient KV cache storage, and compromised model performance, with no method optimizing all three simultaneously.

To address this limitations, we propose **Grouped-head latenT Attention (GTA)**, a novel attention framework that optimizes memory usage and computational efficiency while preserving the expressive power of MHA. GTA introduces two key innovations, as detailed in our method. First, it employs a shared attention map mechanism, grouping query and key projections to reuse computations across heads, thereby reducing computational overhead while maintaining fine-grained attention patterns. Second, it leverages a nonlinear value decoder that compresses the value cache into a compact latent space, using a context-adaptive sigmoid gate to dynamically generate head-specific values [11]. This design, illustrated in our architectural diagrams, significantly reduces memory requirements compared to traditional attention mechanisms, enabling efficient inference without sacrificing model quality. By combining grouped projections with nonlinear decoding, GTA achieves robust expressivity, overcoming the trade-offs observed in GQA and MLA.

In this paper, we show the design roadmap of GTA, and present experiments on GTA models ranging from 160M to 1B parameters. Not only the statistical validation of GTA's efficiency is provided the practical evaluations of cache footprint and latency are also carried out. The contributions of this work are as follows:

- Proposal of GTA, a novel attention mechanism that reduces self-attention computation by up to **62.5%** and KV cache size by up to **70%** while preserving expressive power through shared attention maps and nonlinear decoding.
- Training of GTA models on large-scale corpora and validation of their performance, matching or surpassing GQA on benchmarks across model scales from **160M to 1B** parameters.
- Analysis of GTA's inference speed in prefill and decode stages, demonstrating **2x** throughput compared to GQA, validating its effectiveness for low-latency LLM deployment. By breaking the conventional trade-off between efficiency and expressivity, GTA paves the way for scalable, sustainable, and high-performance LLM deployment in various devices.
- This paper record the attention mechanism design process, including detailed design introduction, analysis methods, and evaluation procedures, guiding future efficient attention designs.

## 2 Related Work

Attention mechanisms are central to LLMs, enabling effective modeling of contextual dependencies [3]. However, the KV cache in standard attention mechanisms scales linearly with sequence length, creating memory and computational bottlenecks [4]. Recent research has developed dense attention variants to optimize KV cache usage through sharing or compression, aligning with GTA. We review these approaches, focusing on methods that share KV caches across heads or layers and those that use latent compression, positioning GTA's contributions.

**Shared KV cache methods.** Several methods reduce memory usage by sharing KV caches across heads or layers. MHA [3], the transformer baseline, uses independent KV caches for each head, resulting in high memory demands. MQA [6] shares a single KV pair across all heads, significantly reducing memory but limiting expressivity. GQA [7] groups heads and shares KV pairs within each group, balancing efficiency and performance, as seen in LLaMA [2]. You Only Cache Once (YOCO) [12] employs a decoder-decoder architecture to cache KV pairs once, sharing them across

layers via cross-attention, reducing memory while maintaining global attention. These methods trade off some expressivity for efficiency, which GTA addresses through its design.

**Latent attention mechanisms.** Another approach compresses the KV cache using latent representations. MLA used in DeepSeek-V3 [8] and PLM [13], compresses keys and values into a latent vector, achieving significant memory savings while preserving performance. Similarly, GTA uses a compressed latent value representation with a nonlinear decoder to generate head-specific values, enhancing expressivity with low computational costs. GTA’s nonlinear decoding, inspired by gated mechanisms like GLU [14] and GLA [15], distinguishes it by maximizing information density.

**Performance-focused attention.** Some methods prioritize performance over efficiency. Multi-Token Attention (MTA) [10] uses convolutions to enhance contextual interactions, and the Differential Transformer [9] employs dual softmax maps for sharper focus. These approaches improve accuracy but often increase computational complexity, unlike GTA’s efficiency-driven design.

**Comparison with [16]** The paper [16] introduces Grouped Tied Attention, which reduces cache requirements by sharing key and value components, thereby increasing arithmetic intensity. Building on this, Grouped Latent Attention is proposed to enhance model parallelism through grouped operations on latent variables within the MLA framework. In contrast, Grouped-Head LatenT Attention (GTA) proposed in this paper adopts a novel attention matrix sharing strategy combined with a nonlinear value decoding process. To our knowledge, this is the first approach to achieve simultaneous improvements in both the prefill and decode phases without compromising model quality.

### 3 Method

In this section, we present our proposed **Grouped-Head Latent Attention (GTA)** mechanism, which enhances the efficiency of transformer architectures while retaining their expressive power. We begin by revisiting Multi-Head Attention (MHA) and introducing our efficiency-driven variants, Grouped-Value Attention (GVA) and Grouped-Head Attention (GHA). These approaches progressively reduce memory and computational overheads but introduce trade-offs in expressivity. Building on their insights, we introduce GTA, which employs a compressed latent representation and a nonlinear decoder to achieve superior efficiency and performance.

#### 3.1 Evolving Patterns of Attention Mechanisms

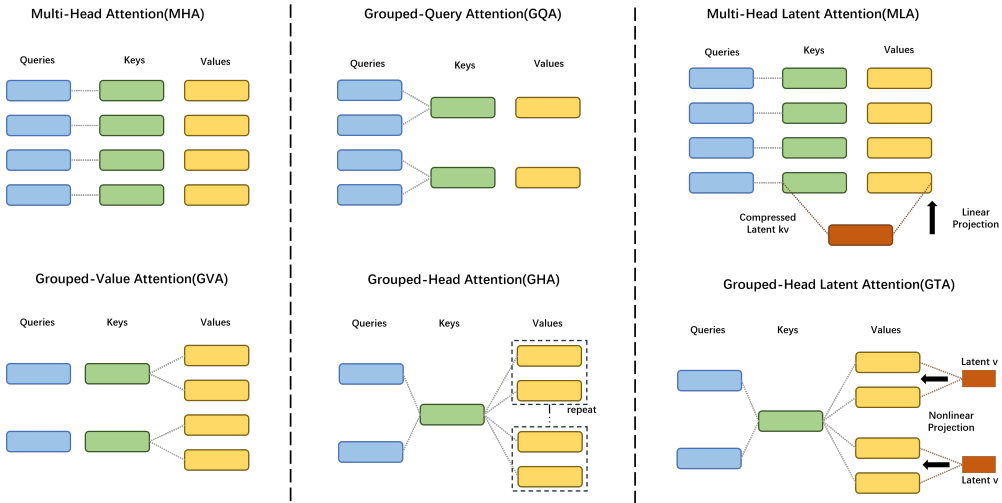


Figure 1: Attention Architecture: Comparing MHA with GVA and GHA, highlighting key, query, and value projection differences. Left-to-right: cache reduction via sharing and compression; top-to-bottom: attention computation reduction via shared attention maps and non-linearity.

**Brief introduction to MHA** MHA [3] underpins modern transformers by enabling the model to attend to diverse sequence patterns. For an input  $X \in \mathbb{R}^{N \times H}$ , where  $N$  denotes sequence length and  $H$  the hidden dimension, MHA projects  $X$  into queries, keys, and values:

$$[Q_1, \dots, Q_{n_h}] = Q = XW_Q \in \mathbb{R}^{N \times n_h d_h}, \quad (1)$$

$$[K_1, \dots, K_{n_h}] = K = XW_K \in \mathbb{R}^{N \times n_h d_h}, \quad (2)$$

$$[V_1, \dots, V_{n_h}] = V = XW_V \in \mathbb{R}^{N \times n_h d_h}, \quad (3)$$

where  $W_Q, W_K, W_V \in \mathbb{R}^{H \times n_h d_h}$  are projection matrices,  $n_h$  is the number of heads, and  $d_h$  satisfies  $n_h \cdot d_h = H$ . Each head computes:

$$O_i = \text{Softmax} \left( \frac{Q_i K_i^T}{\sqrt{d_h}} \right) V_i W_{O_i} \in \mathbb{R}^{N \times H}, \quad (4)$$

with  $W_{O_i} \in \mathbb{R}^{d_h \times H}$  as the output projection, yielding  $O = \sum_{i=1}^{n_h} O_i$ . While effective, MHA’s key-value (KV) cache grows as  $\mathcal{O}(2HN)$ , posing scalability challenges for long sequences.

To address these inefficiencies, techniques such as Multi-Query Attention (MQA) [6] and Grouped-Query Attention (GQA) [7] emerged, reducing memory overhead by sharing keys and values across heads. Building on this foundation, we introduce GVA and GHA as evolutionary steps toward our novel GTA mechanism.

**Grouping Values to Share Attention Matrix** In GVA, the attention weights computed from queries and keys are shared across groups of heads. This means that multiple heads within a group apply the same attention distribution but operate on distinct value projections. By reusing the attention weights, GVA reduces redundant computation while preserving the ability of each head to produce unique outputs through its own value transformation. This strikes a balance between efficiency and representational flexibility, though it still requires maintaining a full set of value projections, keeping memory usage relatively high.

**Grouping Heads to Compress Attention** GHA extends this idea by sharing query and key representations within groups of heads, while deriving distinct value representations for each head. Specifically, multiple heads in a group use the same query and key representations, but their values are computed separately from a shared source, further compressing the memory footprint of the KV cache. This sharing mechanism significantly lowers both computational and storage costs, making GHA well-suited for resource-constrained settings. However, the reduced diversity in query and key representations can limit the model’s ability to capture fine-grained dependencies, potentially impacting performance on complex tasks.

The progression from MHA to GVA and GHA illustrates a critical trade-off between efficiency and expressivity in attention mechanisms. These insights motivate the development of GTA, which introduces a novel nonlinear decoder to achieve greater efficiency without sacrificing performance, addressing the limitations of its predecessors.

### 3.2 Grouped-Head Latent Attention

GHA mitigates the computational and memory demands of MHA by sharing query, key, and value representations across heads, but this often compromises expressivity due to fewer unique representations. To address this limitation, we propose GTA, a novel mechanism that enhances efficiency while preserving representational power. By integrating a compressed latent value representation with a nonlinear decoder, GTA dynamically generates head-specific values, achieving robust expressivity with a reduced memory footprint. This design, illustrated in [Figure 2](#), makes GTA particularly suited for resource-constrained inference.

**Input projections and grouping** GTA begins by processing an input sequence  $X \in \mathbb{R}^{N \times H}$ , where  $N$  is the sequence length and  $H$  is the hidden dimension. It computes queries, keys, and a compressed latent value representation as follows:

$$Q = XW_Q \in \mathbb{R}^{N \times n_q d_h}, \quad K = XW_K \in \mathbb{R}^{N \times n_k d_h}, \quad C = XW_C \in \mathbb{R}^{N \times n_c d_l}, \quad (5)$$

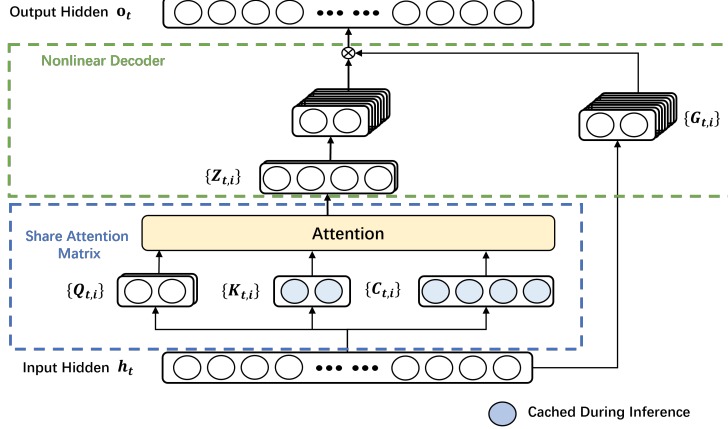


Figure 2: **GTA architecture:** GTA employs a compressed latent value representation  $C$  with dimension  $d_l$ , combined with a nonlinear decoder that uses element-wise multiplication with a sigmoid gate. This design preserves expressive power while reducing the key-value cache size and computational costs compared to traditional attention mechanisms.

where  $W_Q \in \mathbb{R}^{H \times n_q d_h}$ ,  $W_K \in \mathbb{R}^{H \times n_k d_h}$ , and  $W_C \in \mathbb{R}^{H \times n_c d_l}$  are projection matrices. Here,  $n_q$ ,  $n_k$ , and  $n_c$  represent the number of query, key, and value groups, while  $d_h$  and  $d_l$  denote the head and latent dimensions, with  $d_l \geq d_h$  to ensure expressive projections.

To enhance efficiency, GTA organizes these representations into groups. Queries are divided into  $n_q$  groups, with each head  $i$  using  $Q_{q(i)} \in \mathbb{R}^{N \times d_h}$  via a mapping  $q(i)$ . Keys are partitioned into  $n_k$  groups, with head  $i$  accessing  $K_{k(i)} \in \mathbb{R}^{N \times d_h}$  via a mapping  $k(i)$ . Values are derived from the latent representation  $C$ , split into  $n_c$  groups, with head  $i$  using  $C_{c(i)} \in \mathbb{R}^{N \times d_l}$  from group  $c(i)$ . This hierarchical grouping minimizes redundancy, preserves flexible attention patterns, and paves the way for efficient value generation.

**Nonlinear value decoder** Building on this grouped structure, GTA generates head-specific value matrices  $V_i \in \mathbb{R}^{N \times d_h}$  for each head  $i$ :

$$V_i = C_{c(i)} W_{P,i} \odot \text{Sigmoid}(x_t W_{G,i}), \quad (6)$$

where  $W_{P,i} \in \mathbb{R}^{d_l \times d_h}$  is a head-specific projection matrix,  $W_{G,i} \in \mathbb{R}^{H \times d_h}$  is a gating matrix, and  $x_t \in \mathbb{R}^H$  is the current token's representation.

The gate  $\text{Sigmoid}(x_t W_{G,i}) \in \mathbb{R}^{d_h}$ , broadcasting across the sequence, introduces nonlinearity through element-wise multiplication ( $\odot$ ). For each head  $i$ , GTA generates the value  $V_i \in \mathbb{R}^{N \times d_h}$  from the compressed latent representation  $C_{c(i)} \in \mathbb{R}^{N \times d_l}$ , where  $c(i)$  assigns head  $i$  to one of  $n_c$  value groups. The projection is performed using  $W_{P,i} \in \mathbb{R}^{d_l \times d_h}$ , which combines a direct mapping for a subset of  $C_{c(i)}$ 's elements—determined by the head and group assignment—with a learnable component initialized with small random values to enhance diversity. The resulting projection,  $C_{c(i)} W_{P,i}$ , is then modulated by the gate, introducing nonlinearity and enabling context-adaptive feature selection. This design ensures full-rank projections, preventing information loss and enhancing the diversity of the final output across heads within the same group. The nonlinear decoding process thus enables GTA to produce expressive, context-sensitive values for attention computation.

### 3.3 Efficient attention computation

Using the dynamically generated values, GTA computes the attention output for each head  $i$ :

$$O_i = \text{Softmax} \left( \frac{Q_i K_{k(i)}^T}{\sqrt{d_h}} \right) V_i W_{O,i}, \quad (7)$$

where  $W_{O,i} \in \mathbb{R}^{d_h \times H}$  is the output projection, and the final output is  $O = \sum_{i=1}^{n_h} O_i$ . For efficient inference, GTA reformulates the computation:

$$O_i = \left( \text{Softmax} \left( \frac{Q_i K_{k(i)}^T}{\sqrt{d_h}} \right) C_{c(i)} W_{P,i} \right) \odot \text{Sigmoid}(x_t W_{G,i}) W_{O,i}. \quad (8)$$

GTA caches both the compressed latent values  $C \in \mathbb{R}^{N \times n_c d_l}$  and keys  $K \in \mathbb{R}^{N \times n_k d_h}$ , resulting in a memory footprint of  $\mathcal{O}((n_c d_l + n_k d_h)N)$ . This design reduces memory usage compared to traditional grouped attention mechanisms, while computing the nonlinear gate on-the-fly using  $x_t$ , thereby minimizing computational overhead. Furthermore, GTA’s nonlinear decoder enhances expressivity over linear projections by combining a compact latent representation with a context-aware sigmoid gate, improving output diversity, akin to increasing the effective rank [14]. This architecture, illustrated in Figure 2, achieves a robust balance of scalability, expressivity, and efficiency, making GTA a compelling solution for resource-constrained tasks.

## 4 Performance Evaluation

To evaluate the effectiveness of our proposed GTA approach, we conduct extensive experiments on language model pretraining with varying model sizes and sequence lengths. We analyze performance in terms of evaluation loss, parameter count, and memory efficiency of KV cache. Additionally, we perform ablation studies to investigate the impact of specific design choices.

### 4.1 Validating GTA effectiveness

We train transformer language models on the C4 dataset [17] using sequence lengths of 2048 and 4096 tokens. Training employs the AdamW optimizer [18] with cosine scheduler and the TinyLlama tokenizer [19]. Full training details are provided in Appendix A.1 and Appendix A.2. To benchmark our GTA, we compare it against the following attention variants: MHA [3], GQA [7] and MLA [8].

Prior work often adjusts model parameters (e.g., hidden state dimensions) to match total parameter counts across architectures, but this can confound the analysis of attention mechanisms by altering MLP capacity. To isolate the impact of attention, we adopt a framework that fixes non-attention parameters (e.g., hidden state dimensions, MLP sizes) across models, allowing parameter count variations solely due to attention design. This ensures a controlled comparison, focusing on the attention mechanism’s contribution to performance and efficiency.

**Results for 160M parameter models.** Table 1 presents the performance of models with approximately 160M parameters. At a sequence length of 2048 tokens, GTA (with the GTA2 configuration) achieves a lower evaluation loss and better Wikitext perplexity (PPL) compared to MHA, GQA, and MLA. Additionally, GTA (with the GTA1 configuration) records higher downstream task accuracy, demonstrating a notable improvement. These results are achieved using only 12.5% of MHA’s KV cache size per layer (192 vs. 1536 dimensions), highlighting GTA’s memory efficiency. At a sequence length of 4096 tokens, GTA remains competitive, delivering the lowest evaluation loss and comparable PPL, alongside the highest average downstream accuracy. This indicates GTA’s ability to maintain strong performance with reduced memory requirements for longer sequences.

Table 1: Performance of 160M parameter models at sequence lengths of 2048 and 4096. This table compares models based on total parameter count, KV cache dimensions per layer, evaluation loss, and average accuracy across a suite of downstream tasks.

Model	Params	Cache/layer	Seq Len	Eval Loss	Wikitext PPL	PIQA	HellaSwag	ARC-e	ARC-c	Winogrande	Avg
GQA	158.50M	384 (3 $\times$ 2 $\times$ 64)	2048	2.719	23.63	65.94	30.70	42.59	19.53	51.38	42.03
MLA	172.54M	288 (256+32)	2048	2.707	22.69	65.01	30.72	40.65	19.19	51.38	41.39
MHA	178.78M	1536 (12 $\times$ 2 $\times$ 64)	2048	2.696	23.03	66.26	30.87	42.85	17.49	52.17	41.93
GTA1	160.75M	192 (64+128)	2048	2.712	22.67	66.21	30.62	42.63	19.80	52.80	<b>42.41</b>
GTA2	164.13M	192 (64+128)	2048	<b>2.690</b>	<b>22.41</b>	65.72	31.42	41.58	19.45	53.59	42.35
GQA	158.50M	384 (3 $\times$ 2 $\times$ 64)	4096	2.831	26.93	63.71	29.28	39.27	18.26	49.96	40.09
MLA	172.54M	288 (256+32)	4096	2.823	24.98	64.09	29.52	38.89	18.43	50.75	40.33
MHA	178.78M	1536 (12 $\times$ 2 $\times$ 64)	4096	2.827	25.16	63.87	29.38	39.56	18.77	47.67	39.85
GTA1	160.75M	192 (64+128)	4096	2.819	<b>24.01</b>	63.82	29.53	39.48	18.60	52.80	<b>40.85</b>
GTA2	164.13M	192 (64+128)	4096	<b>2.812</b>	25.06	63.71	29.30	38.85	20.48	51.30	40.73

**Results for 500M parameter models.** Table 2 summarizes results for models with approximately 500M parameters. At 2048 tokens, GTA achieves a lower evaluation loss and higher downstream

accuracy, with competitive PPL relative to MHA and GQA. This performance is attained with only 12.5% of MHA’s KV cache size (320 vs. 2560 dimensions). Configurations with smaller caches (e.g., 192 dimensions, 7.5% of MHA’s) yield comparable results, balancing performance and efficiency. At 4096 tokens, GTA not only matches MHA’s evaluation loss but also provides lower Wikitext PPL and higher downstream accuracy. Its reduced memory footprint remains a key benefit.

Table 2: Performance of 500M parameter models at sequence lengths of 2048 and 4096. This table compares models based on total parameter count, KV cache dimensions per layer, evaluation loss, and average accuracy across a suite of downstream tasks.

Model	Params	Cache/layer	Seq Len	Eval Loss	Wikitext PPL	PIQA	HellaSwag	ARC-e	ARC-c	Winogrande	Avg
GQA	483.23M	512 (4 $\times$ 2 $\times$ 64)	2048	2.508	18.52	68.61	34.31	46.72	22.44	51.62	44.73
MLA	516.00M	342 (320+32)	2048	2.486	<b>16.44</b>	68.77	34.52	45.86	19.45	53.43	44.41
MHA	543.27M	2560 (20 $\times$ 2 $\times$ 64)	2048	2.484	17.53	68.44	35.11	47.35	20.73	50.91	44.51
GTA3	486.98M	192 (64+128)	2048	2.503	17.34	68.50	34.22	46.84	19.80	50.28	43.92
GTA4	500.11M	320 (64+256)	2048	<b>2.478</b>	16.82	68.55	34.93	47.05	20.99	53.51	<b>45.01</b>
GQA	483.23M	512 (4 $\times$ 2 $\times$ 64)	4096	2.614	19.01	67.41	31.97	43.86	18.43	52.17	42.77
MLA	516.00M	342 (320+32)	4096	2.596	17.99	65.78	32.29	44.28	19.20	52.88	42.89
MHA	543.27M	2560 (20 $\times$ 2 $\times$ 64)	4096	<b>2.592</b>	19.87	66.65	32.79	43.98	19.37	51.62	42.88
GTA3	486.98M	192 (64+128)	4096	2.609	18.77	67.25	31.85	44.49	18.26	51.07	42.58
GTA4	500.11M	320 (64+256)	4096	<b>2.592</b>	<b>16.96</b>	66.97	32.45	43.94	18.26	53.18	<b>42.96</b>

## 4.2 GTA parameter sensitivity analysis

We perform ablation studies to evaluate the sensitivity of our GTA to critical parameters: attention matrix sharing, head dimension, and nonlinearity choice. Key findings include: (1) sharing attention matrices across heads reduces parameters and slightly improves performance, suggesting a regularization benefit; (2) increasing head dimension enhances performance for both GTA and GQA, with GTA consistently outperforming GQA; and (3) Sigmoid nonlinearity outperforms sparser alternatives (e.g., Silu [20], ReLU<sup>2</sup> [21]), emphasizing the need for higher-rank value representations. Comprehensive results and configurations are detailed in Appendix A.4.

## 4.3 Scaling to 1B language model

To investigate the impact of scaling model size and training data, we train two models, GTA-1B and GQA-1B, each with 1 billion parameters, trained on 220 billion tokens from the smollm-corpus [22] dataset, with details in Appendix A.1. GQA-1B adopts the LLaMA-3.2 [23] framework with MobileLLM’s [24] optimal hyperparameters, tuned via extensive search. GTA-1B, designed for efficiency, uses only 30% of GQA-1B’s cache size while maintaining competitive performance.

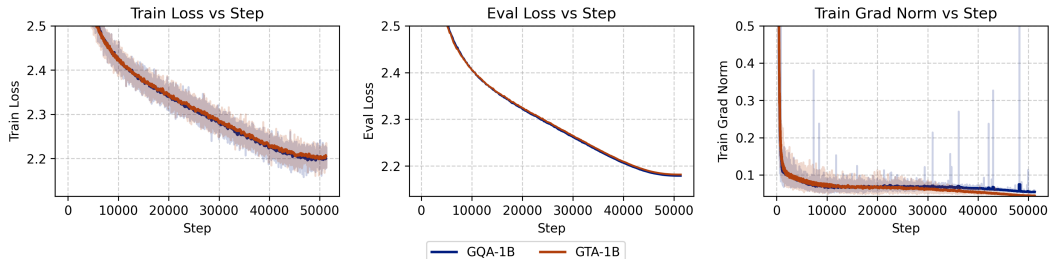


Figure 3: Loss and gradient norm curves over 50,000 training steps for GTA-1B and GQA-1B, showing stable convergence with GTA-1B’s reduced cache size.

Figure 3 shows the training curves, with both models converging stably. GTA-1B’s loss trajectory matches GQA-1B’s, despite its reduced cache, highlighting its memory-efficient architecture. We leverage lm-evaluation-harness [25] to evaluate our models. These evaluation datasets can be divided into: general tasks (ARC-e, ARC-c [26], HellaSwag [27], BoolQ [28], PIQA [29], MathQA [30], TruthfulQA [31], SIQA [32]); coding task (MBPP [33]); instruction following task (IFEval [34]); reasoning tasks (LogiQA [35], BBH [36]);

For supervised fine-tuning (SFT), we further train both base models using the tulu3 dataset [37], a diverse collection of instruction-tuning data designed to enhance model generalization across tasks.

Table 3: We evaluate our models with several common and domain benchmarks, the vertical line denotes different few-shot numbers, where the left ones use 5-shot and the right ones use 3-shot.

Model	PIQA	HellaS.	LogiQA	SIQA	ARC-e	ARC-c	BoolQ	MathQA	TQA	BBH	IFEval	MBPP	Avg.
GQA-1B	75.03	46.46	24.42	46.26	77.02	42.58	63.89	25.56	40.48	23.01	9.90	12.80	<b>40.62</b>
GTA-1B	74.59	46.47	23.50	44.26	75.63	40.87	62.01	25.93	39.01	21.01	9.80	11.60	39.56
GQA-1B-SFT	74.31	45.52	20.58	42.42	70.45	36.09	63.57	26.26	40.89	22.01	29.76	15.80	40.64
GTA-1B-SFT	74.59	45.20	19.80	45.08	71.30	39.16	65.01	26.47	41.30	25.50	36.04	16.60	<b>42.17</b>

The fine-tuned models, GTA-1B-SFT and GQA-1B-SFT, are evaluated on the same benchmarks. **Table 3** shows that GTA-1B-SFT delivers performance comparable to GQA-1B-SFT across diverse benchmarks, with a notable improvement in average accuracy. This competitive performance, combined with GTA-1B’s reduced cache size, highlights its ability to generalize effectively during fine-tuning under resource constraints.

In summary, GTA-1B achieves comparable performance to GQA-1B in both base and fine-tuned settings, using only 30% of GQA-1B’s KV cache size and 37.5% of its self-attention computational cost. These results underscore the potential of memory- and compute-efficient architectures for scaling large language models, enabling sustainable and resource-efficient AI development.

## 5 Efficiency Evaluation

In this section, we evaluate the computational and memory efficiency of our GTA mechanism against prominent attention variants: MHA, GQA, MLA, GVA, and GHA. Through theoretical analysis and empirical benchmarks, we demonstrate GTA’s ability to achieve high expressivity with reduced resource demands, positioning it as an efficient solution for modern transformer architectures.

### 5.1 Theoretical efficiency analysis

**Table 4** compares the key-value (KV) cache size and computational complexity across attention mechanisms, with detailed analysis provided in Appendix B. GTA achieves a KV cache size of  $(n_k d_h + n_c d_l)N$ , significantly smaller than MHA’s  $2n_h d_h N$ . Its attention computation,  $n_q(d_h + d_l)N^2$ , is also lower than MHA’s  $2n_h d_h N^2$ , enhancing inference efficiency. While GTA introduces additional linear computation, this trade-off substantially improves model expressivity, rivaling MHA while maintaining efficiency comparable to GVA and GHA.

Table 4: Comparison of computational complexity and memory requirements for different attention mechanisms.  $H$  is the hidden dimension,  $N$  is the sequence length,  $n_q, n_k, n_v, n_c$  are the number of query, key, value, and latent value heads, respectively,  $d_h$  is the per-head dimension, and  $d_l$  is the latent dimension.

Attention	KV Cache per Layer	Attention	Computation per Layer		Expressivity
			Linear		
<b>MHA</b>	$2n_h d_h N$	$2n_h d_h N^2$		$4NH^2$	Strong
<b>GQA</b>	$2n_h d_h N$	$2n_h d_h N^2$		$2NH^2 + 2n_k d_h NH$	Moderate
<b>MLA</b>	$(d_c + d_{rope})N$	$n_h(d_{rope} + 2d_{nope})N^2$	$((d_c + d_{rope})H + n_h(d_{rope} + d_{nope})H + 2n_h d_l d_{nope} + H^2)N$		Strong
<b>GVA</b>	$(H + n_k d_h)N$	$(n_q d_h + n_h d_h)N^2$		$2NH^2 + 2n_k d_h NH$	Moderate
<b>GHA</b>	$(n_k d_h + n_v d_h)N$	$(n_q d_h + n_h d_h)N^2$		$NH^2 + n_q d_h NH + n_k d_h NH + n_v d_h NH$	Weak
<b>GTA (Ours)</b>	$(n_k d_h + n_c d_l)N$	$n_q(d_k + d_l)N^2$	$2NH^2 + (n_q d_h + n_k d_h + n_c d_l + d_l)NH$		Strong

As shown in **Table 4**, GTA achieves substantial efficiency gains in both computation and memory usage. The KV cache size is reduced from  $2HN$  in MHA to  $(n_k d_h + n_c d_l)N$ , where  $n_k \ll n_h$  and  $n_c \ll n_h$ . This translates to a reduction factor of approximately  $\frac{2H}{n_k d_h + n_c d_l}$ , which can be significant for large models. The attention computation is also reduced from  $2n_h d_h N^2$  to  $n_q(d_h + d_l)N^2$ , offering proportional speedups during inference.

### 5.2 Conducting empirical benchmarks via LLM-Viewer [38]

To substantiate the theoretical advantages, we benchmark GTA-1B against GQA-1B using the LLM-Viewer framework on an NVIDIA H100 80GB GPU. This framework simulates optimal inference performance based on hardware specifications and model configurations. **Figure 4** illustrates

the prefill and decode times across various configurations. GTA-1B consistently outperforms GQA-1B in both compute-bound prefill and I/O-bound decode phases, demonstrating superior latency characteristics. More hardware and detailed evaluation results are provided in Appendix C.

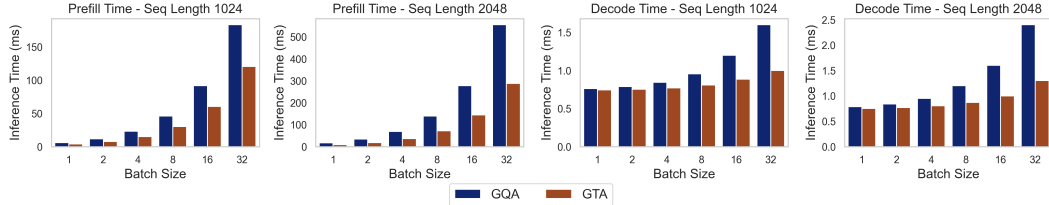


Figure 4: Prefill and decode times for GTA-1B and GQA-1B across configurations on an NVIDIA H100 80GB GPU. GTA-1B achieves lower latency in both compute-bound prefill and I/O-bound decode phases, showcasing its enhanced efficiency.

### 5.3 Deployment in Practice

Refer to PLM [13], to assess the real-world performance of GTA-1B, we conduct inference experiments using the `transformers` library, measuring prefill and decode times across a diverse set of hardware platforms: NVIDIA H100 (server-grade GPU), NVIDIA A800 (server-grade GPU), RTX 3060 (consumer-grade GPU), Apple M2 (ARM-based processor), and BCM2712 (mobile processor). This approach enables direct measurement of real-world inference latency, capturing hardware-specific optimizations and system-level overheads, in contrast to the theoretical simulations provided by LLM-Viewer.

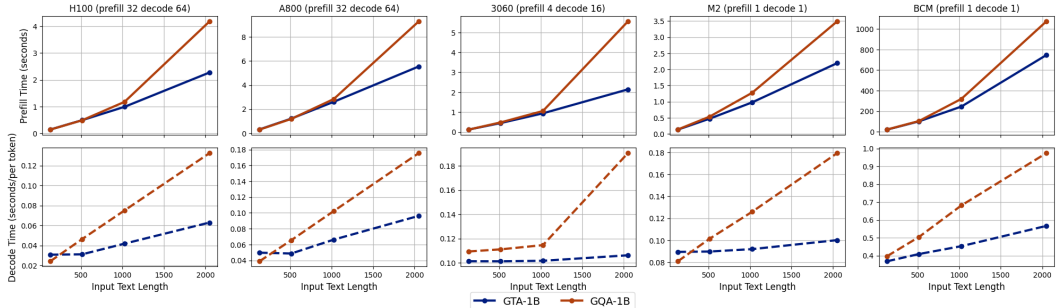


Figure 5: Comparison of prefill (top row) and decode (bottom row) times for GTA-1B and GQA-1B across various configurations on NVIDIA H100, NVIDIA A800, RTX 3060, Apple M2, and BCM2712. Prefill plots (top) display input text length on the x-axis and time required on the y-axis. Decode plots (bottom) show starting generation length on the x-axis and time to generate 128 tokens on the y-axis.

As illustrated in Figure 5, GTA-1B (blue solid line) consistently outperforms GQA-1B (orange dashed line) in prefill times across all tested platforms, with the performance gap widening at longer input lengths, such as 2k tokens. For instance, on the NVIDIA A800, GTA-1B demonstrates a significant reduction in prefill times compared to GQA-1B at 2k tokens. During the decode phase, GTA-1B also exhibits superior performance, particularly at extended generation lengths, a pattern that holds across all hardware types, underscoring its robustness.

Figure 6 showcases the performance with cache offload enabled. On the NVIDIA H100, GTA-1B sustains its prefill advantage at longer input lengths and delivers even greater improvements in decode times compared to GQA-1B. This consistent trend across all platforms highlights GTA-1B's efficiency in I/O-bound scenarios, where cache offload necessitates frequent data transfers between GPU and CPU memory.

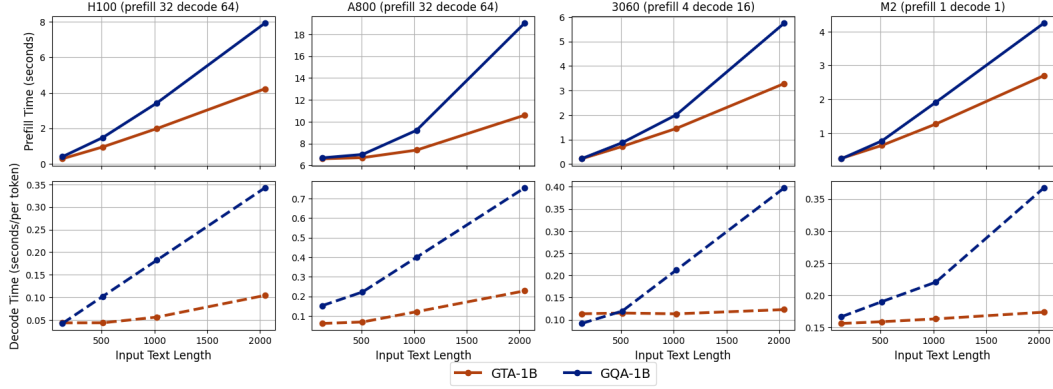


Figure 6: Performance comparison of GTA-1B and GQA-1B with cache offload enabled, showing prefill (top row) and decode (bottom row) times on NVIDIA H100, NVIDIA A800, RTX 3060, Apple M2, and BCM2712. Prefill plots (top) present input text length (x-axis) versus time (y-axis); decode plots (bottom) present starting generation length (x-axis) versus time to generate 128 tokens (y-axis). Cache offload transfers the key-value cache to CPU memory to alleviate GPU memory constraints, resulting in I/O-bound conditions due to frequent data transfers.

Batch sizes for prefill and decode are customized to reflect realistic usage scenarios for each hardware type. For server-grade GPUs like the NVIDIA H100 and A800, designed for high-throughput server environments, we use a prefill batch size of 32 and a decode batch size of 64 to emulate large-scale demand. For consumer-grade devices such as the Apple M2 and BCM2712, typically employed by individual users, both prefill and decode batch sizes are set to 1. For the RTX 3060, a consumer-grade GPU often handling moderate multi-user workloads alongside other tasks, we select a prefill batch size of 4 and a decode batch size of 16 to represent a balanced scenario.

In summary, GTA-1B surpasses GQA-1B in both prefill and decode times across diverse hardware platforms, with notable advantages at longer input lengths. It excels in standard inference settings and I/O-bound conditions with cache offload, demonstrating versatility across varying hardware capabilities and batch sizes. This adaptability positions GTA-1B as a practical solution for both server-grade and consumer-grade deployments, enhancing the efficiency of attention mechanisms in large language models by reducing computational complexity and memory demands.

Further details on the experimental setup, including comprehensive hardware specifications and test configurations, are available in Appendix C.2.

In summary, GTA-1B demonstrates a balanced combination of memory efficiency, computational speed, and practical performance, as evidenced by its competitive inference speeds in `transformers`-based experiments. Notably, GTA-1B retains the same MLP design as the baseline model, ensuring that the observed performance gains are attributable to the novel attention mechanism rather than changes in the MLP. The results validate the trends observed in `LLM-Viewer` benchmarks, reinforcing GTA-1B’s scalability and suitability for real-world deployment of modern transformer architectures.

## 6 Conclusion

We present Grouped-head Latent Attention (GTA), which shares attention maps across heads and encodes values in a learned latent space to exploit redundancy. GTA reduces attention FLOPs by up to 62.5% and reduce KV cache size by up to 70% compared to GQA, matching perplexity while doubling inference speed on commodity hardware. By seeking the trade-off between efficiency and expressivity, GTA enables efficient LLM design and deployments across a wide range of real-world scenarios. The limitation stems from our lack of engineering-focused optimization efforts, which prevents us from achieving the theoretical upper bound of efficiency gains.

## References

- [1] Tom Brown, Benjamin Mann, Nick Ryder, Melanie Subbiah, Jared D Kaplan, Prafulla Dhariwal, Arvind Neelakantan, Pranav Shyam, Girish Sastry, Amanda Askell, et al. Language models are few-shot learners. *Advances in neural information processing systems*, 33:1877–1901, 2020.
- [2] Hugo Touvron, Thibaut Lavril, Gautier Izacard, Xavier Martinet, Marie-Anne Lachaux, Timothée Lacroix, Baptiste Rozière, Naman Goyal, Eric Hambro, Faisal Azhar, et al. Llama: Open and efficient foundation language models. *arXiv preprint arXiv:2302.13971*, 2023.
- [3] Ashish Vaswani, Noam Shazeer, Niki Parmar, Jakob Uszkoreit, Llion Jones, Aidan N Gomez, Łukasz Kaiser, and Illia Polosukhin. Attention is all you need. *Advances in neural information processing systems*, 30, 2017.
- [4] Tri Dao, Dan Fu, Stefano Ermon, Atri Rudra, and Christopher Ré. Flashattention: Fast and memory-efficient exact attention with io-awareness. *Advances in neural information processing systems*, 35:16344–16359, 2022.
- [5] Nelson F. Liu, Kevin Lin, John Hewitt, Ashwin Paranjape, Michele Bevilacqua, Fabio Petroni, and Percy Liang. Lost in the middle: How language models use long contexts, 2023.
- [6] Noam Shazeer. Fast transformer decoding: One write-head is all you need. *arXiv preprint arXiv:1911.02150*, 2019.
- [7] Joshua Ainslie, James Lee-Thorp, Michiel De Jong, Yury Zemlyanskiy, Federico Lebrón, and Sumit Sanghai. Gqa: Training generalized multi-query transformer models from multi-head checkpoints. *arXiv preprint arXiv:2305.13245*, 2023.
- [8] Aixin Liu, Bei Feng, Bing Xue, Bingxuan Wang, Bochao Wu, Chengda Lu, Chenggang Zhao, Chengqi Deng, Chenyu Zhang, Chong Ruan, et al. Deepseek-v3 technical report. *arXiv preprint arXiv:2412.19437*, 2024.
- [9] Tianzhu Ye, Li Dong, Yuqing Xia, Yutao Sun, Yi Zhu, Gao Huang, and Furu Wei. Differential transformer, 2025.
- [10] Olga Golovneva, Tianlu Wang, Jason Weston, and Sainbayar Sukhbaatar. Multi-token attention, 2025.
- [11] Noam Shazeer. Glu variants improve transformer, 2020.
- [12] Yutao Sun, Li Dong, Yi Zhu, Shaohan Huang, Wenhui Wang, Shuming Ma, Quanlu Zhang, Jianyong Wang, and Furu Wei. You only cache once: Decoder-decoder architectures for language models. *Advances in Neural Information Processing Systems*, 37:7339–7361, 2024.
- [13] Cheng Deng, Luoyang Sun, Jiwen Jiang, Yongcheng Zeng, Xinjian Wu, Wenxin Zhao, Qingfa Xiao, Jiachuan Wang, Haoyang Li, Lei Chen, Lionel M. Ni, Haifeng Zhang, and Jun Wang. Plm: Efficient peripheral language models hardware-co-designed for ubiquitous computing, 2025.
- [14] Noam Shazeer. Glu variants improve transformer. *arXiv preprint arXiv:2002.05202*, 2020.
- [15] Songlin Yang, Bailin Wang, Yikang Shen, Rameswar Panda, and Yoon Kim. Gated linear attention transformers with hardware-efficient training, 2024.
- [16] Ted Zadouri, Hubert Strauss, and Tri Dao. Hardware-efficient attention for fast decoding, 2025.
- [17] Colin Raffel, Noam Shazeer, Adam Roberts, Katherine Lee, Sharan Narang, Michael Matena, Yanqi Zhou, Wei Li, and Peter J. Liu. Exploring the limits of transfer learning with a unified text-to-text transformer, 2023.
- [18] Ilya Loshchilov and Frank Hutter. Decoupled weight decay regularization. *arXiv preprint arXiv:1711.05101*, 2017.
- [19] Peiyuan Zhang, Guangtao Zeng, Tianduo Wang, and Wei Lu. Tinyllama: An open-source small language model. *arXiv preprint arXiv:2401.02385*, 2024.

[20] Stefan Elfwing, Eiji Uchibe, and Kenji Doya. Sigmoid-weighted linear units for neural network function approximation in reinforcement learning, 2017.

[21] Zhengyan Zhang, Yixin Song, Guanghui Yu, Xu Han, Yankai Lin, Chaojun Xiao, Chenyang Song, Zhiyuan Liu, Zeyu Mi, and Maosong Sun. Relu<sup>2</sup> wins: Discovering efficient activation functions for sparse llms, 2024.

[22] Loubna Ben Allal, Anton Lozhkov, Guilherme Penedo, Thomas Wolf, and Leandro von Werra. Smollm-corpus, 2024.

[23] Meta llama team. The llama 3 herd of models, 2024.

[24] Zechun Liu, Changsheng Zhao, Forrest Iandola, Chen Lai, Yuandong Tian, Igor Fedorov, Yunyang Xiong, Ernie Chang, Yangyang Shi, Raghuraman Krishnamoorthi, Liangzhen Lai, and Vikas Chandra. Mobilellm: Optimizing sub-billion parameter language models for on-device use cases, 2024.

[25] Leo Gao, Jonathan Tow, Baber Abbasi, Stella Biderman, Sid Black, Anthony DiPofi, Charles Foster, Laurence Golding, Jeffrey Hsu, Alain Le Noac'h, Haonan Li, Kyle McDonell, Niklas Muennighoff, Chris Ociepa, Jason Phang, Laria Reynolds, Hailey Schoelkopf, Aviya Skowron, Lintang Sutawika, Eric Tang, Anish Thite, Ben Wang, Kevin Wang, and Andy Zou. The language model evaluation harness, 07 2024.

[26] Peter Clark, Isaac Cowhey, Oren Etzioni, Tushar Khot, Ashish Sabharwal, Carissa Schoenick, and Oyvind Tafjord. Think you have solved question answering? try arc, the ai2 reasoning challenge. *arXiv:1803.05457v1*, 2018.

[27] Rowan Zellers, Ari Holtzman, Yonatan Bisk, Ali Farhadi, and Yejin Choi. Hellaswag: Can a machine really finish your sentence? In *Proceedings of the 57th Annual Meeting of the Association for Computational Linguistics*, 2019.

[28] Christopher Clark, Kenton Lee, Ming-Wei Chang, Tom Kwiatkowski, Michael Collins, and Kristina Toutanova. Boolq: Exploring the surprising difficulty of natural yes/no questions. *arXiv preprint arXiv:1905.10044*, 2019.

[29] Yonatan Bisk, Rowan Zellers, Ronan Le Bras, Jianfeng Gao, and Yejin Choi. Piqa: Reasoning about physical commonsense in natural language. In *Thirty-Fourth AAAI Conference on Artificial Intelligence*, 2020.

[30] Aida Amini, Saadia Gabriel, Shanchuan Lin, Rik Koncel-Kedziorski, Yejin Choi, and Hannaneh Hajishirzi. MathQA: Towards interpretable math word problem solving with operation-based formalisms. In *Proceedings of the 2019 Conference of the North American Chapter of the Association for Computational Linguistics: Human Language Technologies, Volume 1 (Long and Short Papers)*, pages 2357–2367, Minneapolis, Minnesota, June 2019. Association for Computational Linguistics.

[31] Stephanie Lin, Jacob Hilton, and Owain Evans. Truthfulqa: Measuring how models mimic human falsehoods, 2022. URL <https://arxiv.org/abs/2109.07958>, 2021.

[32] Maarten Sap, Hannah Rashkin, Derek Chen, Ronan LeBras, and Yejin Choi. Socialqa: Commonsense reasoning about social interactions. *arXiv preprint arXiv:1904.09728*, 2019.

[33] Jacob Austin, Augustus Odena, Maxwell Nye, Maarten Bosma, Henryk Michalewski, David Dohan, Ellen Jiang, Carrie Cai, Michael Terry, Quoc Le, et al. Program synthesis with large language models. *arXiv preprint arXiv:2108.07732*, 2021.

[34] Jeffrey Zhou, Tianjian Lu, Swaroop Mishra, Siddhartha Brahma, Sujoy Basu, Yi Luan, Denny Zhou, and Le Hou. Instruction-following evaluation for large language models. *arXiv preprint arXiv:2311.07911*, 2023.

[35] Jian Liu, Leyang Cui, Hanmeng Liu, Dandan Huang, Yile Wang, and Yue Zhang. Logiqa: A challenge dataset for machine reading comprehension with logical reasoning. *arXiv preprint arXiv:2007.08124*, 2020.

- [36] Mirac Suzgun, Nathan Scales, Nathanael Schärli, Sebastian Gehrmann, Yi Tay, Hyung Won Chung, Aakanksha Chowdhery, Quoc V Le, Ed H Chi, Denny Zhou, et al. Challenging big-bench tasks and whether chain-of-thought can solve them. *arXiv preprint arXiv:2210.09261*, 2022.
- [37] Nathan Lambert, Jacob Morrison, Valentina Pyatkin, Shengyi Huang, Hamish Ivison, Faeze Brahman, Lester James V. Miranda, Alisa Liu, Nouha Dziri, Shane Lyu, Yuling Gu, Saumya Malik, Victoria Graf, Jena D. Hwang, Jiangjiang Yang, Ronan Le Bras, Oyvind Tafjord, Chris Wilhelm, Luca Soldaini, Noah A. Smith, Yizhong Wang, Pradeep Dasigi, and Hannaneh Hajishirzi. Tülu 3: Pushing frontiers in open language model post-training. 2024.
- [38] Zhihang Yuan, Yuzhang Shang, Yang Zhou, Zhen Dong, Chenhao Xue, Bingzhe Wu, Zhikai Li, Qingyi Gu, Yong Jae Lee, Yan Yan, Beidi Chen, Guangyu Sun, and Kurt Keutzer. Llm inference unveiled: Survey and roofline model insights, 2024.
- [39] Yaowei Zheng, Richong Zhang, Junhao Zhang, Yanhan Ye, Zheyan Luo, Zhangchi Feng, and Yongqiang Ma. Llamafactory: Unified efficient fine-tuning of 100+ language models. In *Proceedings of the 62nd Annual Meeting of the Association for Computational Linguistics (Volume 3: System Demonstrations)*, Bangkok, Thailand, 2024. Association for Computational Linguistics.
- [40] Jianlin Su, Murtadha Ahmed, Yu Lu, Shengfeng Pan, Wen Bo, and Yunfeng Liu. Roformer: Enhanced transformer with rotary position embedding. *Neurocomputing*, 568:127063, 2024.

## A Training Detail

### A.1 Pretrain Detail

This section provides a comprehensive overview of the pretraining configurations and procedures employed in our experiments. We detail the model hyperparameters, data settings, and training specifics to ensure reproducibility and provide further insights into our methodology. The experiments were conducted on 4 nodes, each equipped with 8 NVIDIA A800 GPUs (80GB memory), totaling 32 GPUs for distributed training.

**Hardware Configuration** Our training infrastructure consisted of 4 computing nodes, with each node containing 8 NVIDIA A800 GPUs (80GB memory). The distributed training setup allowed flexible allocation of GPU resources, scaling from single-node (8 GPUs) to full-cluster (32 GPUs) configurations depending on model size and training requirements.

**Model hyperparameters** The key architectural hyperparameters for our models are summarized in [Table 5](#). We present configurations for both the 160M and 500M parameter models, highlighting the variations across different attention mechanisms: MHA, MLA, GQA, and our proposed GTA variants.

Table 5: Model hyperparameters

	160M				500M				1B		
	MHA	MLA	GQA	GTA1	MHA	MLA	GQA	GTA3	GTA4	GQA-1B	GTA-1B
<b>Number of layers</b>	24	24	24	24	24	24	24	24	24	54	54
<b>Hidden Dimension</b>	768	768	768	768	1280	1280	1280	1280	1280	1280	1280
<b>Intermediate Size</b>	1920	1920	1920	1920	3584	3584	3584	3584	3584	3584	3584
<b>Number of Attention Heads</b>	12	12	12	12	20	20	20	20	20	20	20
Number of Q Heads	12	12	12	3	6	20	20	5	10	20	5
Number of V Heads	12	1	3	1	1	20	1	4	1	2	1
Number of K Heads	12	1	3	1	1	20	1	4	1	1	5
KV Lora Rank	—	256	—	—	—	320	—	—	—	—	—
Compressed V Head Dimension	—	—	—	128	128	—	—	128	128	—	128
Vocabulary Size	32000	32000	32000	32000	32000	32000	32000	32000	32000	128256	128256
Activation Function	silu										
Tie Embedding Params(M)	TRUE	TRUE	TRUE	TRUE	TRUE	FALSE	FALSE	FALSE	FALSE	TRUE	TRUE
	178.78	172.54	158.50	160.75	164.13	543.27	516.00	483.23	486.98	500.11	1076.38
											1076.48

**Data and hyperparameters** [Table 6](#) details the key hyperparameters used in our pretraining experiments. We employed two different scaling configurations, referred to as "Validation" and "Scaling", to assess the impact of model and data scaling on performance. These configurations differ primarily in global batch size, learning rate, and certain Adam optimizer settings.

Table 6: Experiments hyperparameters.

Hyperparameter	Validation	Scaling	SFT
Global Batch Size	800	2048	96
Learning Rate	2.00E-04	1.00E-03	2.00E-5
Learning Rate Scheduler	cosine	cosine	cosine
Warm up rate	0.01	0.01	0.1
Weight Decay	default(0.0)	0.1	0.1
Adam $\beta_1$	default(0.9)	0.9	0.9
Adam $\beta_2$	default(0.999)	0.95	0.95
Clip Grad	1.0	1.0	1.0
Rms Norm Eps	default(1e-06)	1e-5	1e-5
Attention Dropout	0	0	0
Hidden Dropout	0	0	0
Epoch	1	1	4

### A.2 Loss Curve

To provide insights into the training dynamics, we present the loss curves for various model configurations. [Figure 7](#), [Figure 8](#), [Figure 9](#) and [Figure 10](#) illustrate the training and evaluation loss trajectories for the 160M and 500M models across different sequence lengths. Notably, the evaluation loss is

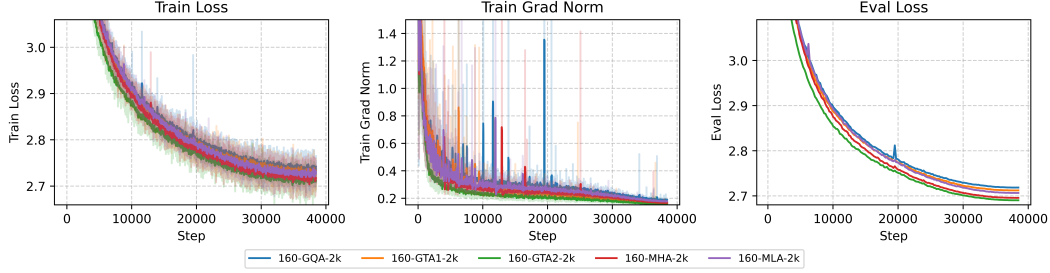


Figure 7: Loss Curve for 160M with 2048 sequence length

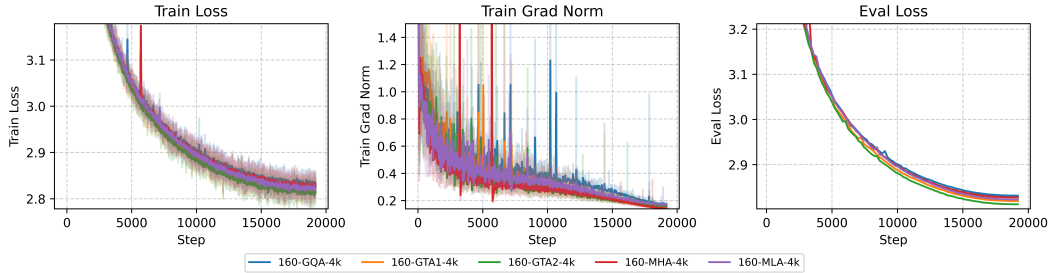


Figure 8: Loss Curve for 160M with 4096 sequence length

slightly lower than the training loss, which can be attributed to the evaluation being conducted on a subset of the data for efficiency, potentially comprising a simpler distribution.

### A.3 SFT Detail

In the SFT stage, we trained our model using the `tulu-3-sft-mixture` [37] dataset. We utilized the LlamaFactory [39] framework with nearly all default hyperparameters. Additional training details are available in [Table 6](#).

### A.4 Sensitivity Analysis Result

**Impact of Shared Attention Matrix** To understand the importance of sharing attention matrix across heads in our GTA architecture, we conduct an ablation study comparing shared vs. non-shared attention matrix. As shown in [Table 7](#), while sharing attention matrix reduces the parameter count from 511.37M to 492.61M, it actually improves performance slightly (2.4995 vs. 2.496). This suggests that our approach not only saves memory and computation but also provides a beneficial

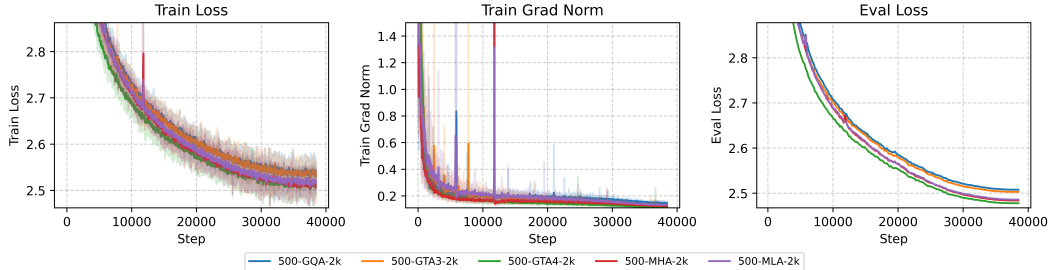


Figure 9: Loss Curve for 500M with 2048 sequence length

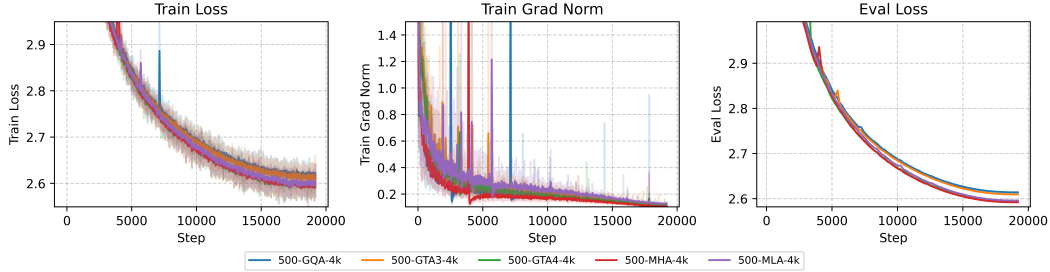


Figure 10: Loss Curve for 500M with 4096 sequence length

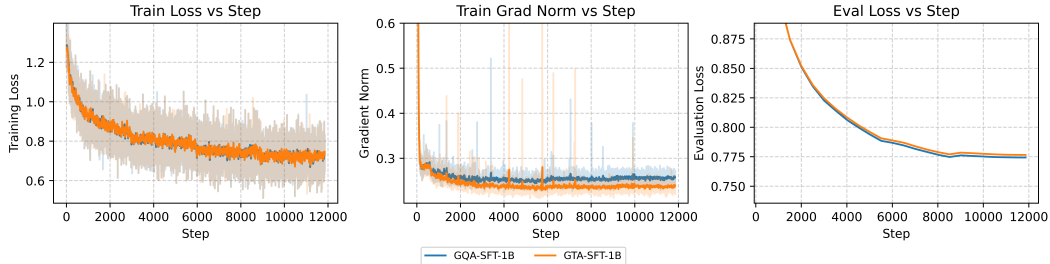


Figure 11: Loss curve for SFT

regularization effect, supporting the hypothesis that traditional attention mechanisms may be over-parameterized.

Table 7: Ablation study on the effect of sharing attention matrix in GTA models (500M parameter range).

Configuration	Parameters	Eval Loss	Cache/layer	Seq Length
GTA with 5 attention matrix groups	486.98M	2.5031	192 (64+128)	2048
GTA with 10 attention matrix groups	492.61M	2.4995	192 (64+128)	2048
GTA without attention matrix groups	511.37M	<b>2.4960</b>	192 (64+128)	2048

**Effect of Head Dimension** We also investigate the effect of increasing the head dimension while keeping the total parameter count similar. Table 9 compares models with head dimensions of 64 and 128. Doubling the head dimension improves performance in both GQA and GTA models, with GTA consistently outperforming GQA. Notably, GTA with doubled head dimensions achieves our best performance (2.492), suggesting that allocating more capacity to each head while sharing attention matrixs is an effective design choice for attention mechanisms.

Table 8: Ablation study on the effect of head dimension in GQA and GTA models (500M parameter range).

Model	Head Dim	Parameters	Head Dim	Eval Loss	Cache/layer	Seq Length
GQA	64	483.23M	64	2.5079	512 (4×2×64)	2048
GTA	64	492.61M	64	<b>2.4995</b>	192 (64+128)	2048
GQA	128	483.23M	128	2.5038	512 (2×2×128)	2048
GTA	128	498.24M	128	<b>2.4844</b>	384 (128+256)	2048

**Choice of Nonlinearity** We explored different nonlinear activation functions for the gating mechanism, including ReLU<sup>2</sup>, Silu, and Sigmoid, and observed that performance degrades as the sparsity of the activation increases. Sigmoid, with its smooth and bounded output, consistently outperformed sparser alternatives like Silu and ReLU<sup>2</sup>, which introduce more zeros and reduce the effective rank

of the value representation. This behavior contrasts with typical MLP architectures, where sparse activations like ReLU often enhance performance by promoting feature selectivity. In GTA, however, the reduced rank caused by sparsity impairs the expressivity of value, underscoring the importance of maintaining a higher rank in the value representation for effective attention computation.

Table 9: Ablation study on the effect of activation function in GTA models (500M parameter range).

Model	Parameters	Activation	Eval Loss	Cache/layer	Seq Length
GTA	492.61M	Sigmoid	<b>2.4995</b>	192 (64+128)	2048
GTA	492.61M	Silu	2.5314	192 (64+128)	2048
GTA	492.61M	ReLU <sup>2</sup>	2.5502	192 (64+128)	2048

## B Computational Analysis

This appendix analyzes the computational costs of GTA, MLA, and GQA.

### B.1 GTA

#### B.1.1 Definition

Let  $\mathbf{h}_t \in \mathbb{R}^H$  represent the input hidden state for the  $t$ -th token in the attention mechanism. The grouped key and compressed value for the  $j$ -th head are denoted by  $\mathbf{k}_{t,j} \in \mathbb{R}^{d_h}$  and  $\mathbf{c}_{t,j} \in \mathbb{R}^{d_c}$ , respectively. The position-independent query for the  $k$ -th head is represented as  $\mathbf{q}_{t,k} \in \mathbb{R}^{d_h}$ . The computations for the attention mechanism proceed as follows:

$$\mathbf{k}_{t,j} = \text{RoPE}(W_{K,j}\mathbf{h}_t), \quad (9)$$

$$\mathbf{q}_{t,k} = \text{RoPE}(W_{Q,k}\mathbf{h}_t), \quad (10)$$

$$\mathbf{v}_{t,j}^C = W_{V,j}\mathbf{h}_t, \quad (11)$$

where  $W_{K,j} \in \mathbb{R}^{d_h \times d}$  and  $W_{C,j} \in \mathbb{R}^{d_h \times d}$  are the up-projection matrices for grouped key and compressed value for the  $j$ -th kv head, and  $W_{Q,k} \in \mathbb{R}^{d_h \times d}$  for the  $k$ -th head, respectively.

The attention outputs  $\{\mathbf{o}_{t,i}\}$  are calculated as follows:

$$\mathbf{o}_{t,i} = \left( \sum_{k=1}^t \text{Softmax}_k \left( \frac{\mathbf{q}_{t,Q(i)}^\top \mathbf{k}_{k,K(i)}}{\sqrt{d_h}} \right) \mathbf{v}_{k,V(i)} \right) W_{P,i}, \quad (12)$$

where  $W_{P,i} \in \mathbb{R}^{d_h \times d_c}$  is the attention projection matrix.

The  $i$ -th head gate  $\mathbf{g}_{t,i} \in \mathbb{R}^{d_h \times H}$  is proceed as follows:

$$\mathbf{g}_{t,i} = W_{G,i}\mathbf{h}_t, \quad (13)$$

The final output is obtained by combining the attention results from all heads through a linear projection:

$$\mathbf{u}_t = W_O [\mathbf{o}_{t,1} \odot \mathbf{g}_{t,1}; \mathbf{o}_{t,2} \odot \mathbf{g}_{t,2}; \dots; \mathbf{o}_{t,n_h} \odot \mathbf{g}_{t,n_h}], \quad (14)$$

where  $W_O \in \mathbb{R}^{d \times d_{\text{hope}} n_h}$  is the output projection matrix and  $n_h$  is the number of attention heads.

#### B.1.2 Prefill

For an input sequence of length  $N$ , the computational complexity begins with the projection operations for keys  $\mathbf{k}_{t,j}$  and compressed values  $\mathbf{c}_{t,j}$ , requiring  $\mathcal{O}(d_h NH)$  and  $\mathcal{O}(d_c NH)$  operations. The query projection  $\mathbf{q}_{t,k}$  further contributes  $\mathcal{O}(d_h NH)$ . The gate projection requires  $\mathcal{O}(NH^2)$  and the attention projection for each head requires  $\mathcal{O}(d_h d_c N)$ . The output projection requires  $\mathcal{O}(NH^2)$ .

Respectively. Aggregating these components, the total linear projection cost becomes:

$$\mathcal{O}(2NH^2 + (n_q d_h + n_k d_h + n_v d_c + d_c)NH).$$

The attention mechanism's computational complexity arises from pairwise interactions between sequence elements, resulting in a quadratic scaling with sequence length  $N$ . Computing attention scores  $QK^T$  has a complexity of  $\mathcal{O}(n_q d_h N^2)$ . Generating the attention output by values  $V$  adds  $\mathcal{O}(n_q d_c N^2)$ . The total complexity is thus  $\mathcal{O}(n_q (d_h + d_c) N^2)$ .

Combining all terms, the total computational complexity for the prefill phase is:

$$\text{Prefill}_{GTA} = \mathcal{O}(2NH^2 + (n_q d_h + n_k d_h + n_v d_c + d_c)NH + n_q (d_h + d_c) N^2).$$

### B.1.3 Decode

For an input sequence of length  $N - 1$ , the decoder phase computes the  $N$ -th token's representations through successive transformations. Key and value projections  $\mathbf{k}_{N,j}$  and  $\mathbf{c}_{N,j}$  require  $\mathcal{O}(d_h H)$  and  $\mathcal{O}(d_c H)$  operations, while the query projection  $\mathbf{q}_{N,i}$  incurs  $\mathcal{O}(d_h H)$ . The gate projection requires  $\mathcal{O}(H^2)$  and the attention projection for each head requires  $\mathcal{O}(d_h d_c)$ . The output projection requires  $\mathcal{O}(H^2)$ . The total computational linear projection cost:

$$\mathcal{O}(2H^2 + (n_q d_h + n_k d_h + n_v d_c + d_c)H).$$

The attention mechanism, operating over cached historical states, scales as  $\mathcal{O}(2n_h d_h N)$ , reflecting linear dependence on sequence length  $N$ . Aggregating all components, the total computational cost is:

$$\text{Generate}_{\text{GTA}} = \mathcal{O}(2H^2 + (n_q d_h + n_k d_h + n_v d_c + d_c)H + 2n_h d_h N).$$

Caching historical keys  $\{\mathbf{k}_{t,j}\}$  and values  $\{\mathbf{v}_{t,j}\}$  for  $t = 1, \dots, N - 1$  demands memory:

$$\text{Cache}_{\text{GTA}} = (n_k d_h + n_v d_c)N,$$

## B.2 MLA

### B.2.1 Definition

Let  $\mathbf{h}_t \in \mathbb{R}^H$  represent the input hidden state for the  $t$ -th token in the attention mechanism. The low-rank key-value joint compression state is denoted as  $\mathbf{c}_t^{KV} \in \mathbb{R}^{d_c}$ , while the decompressed key and value for the  $i$ -th head are denoted by  $\mathbf{k}_{t,i}^C \in \mathbb{R}^{d_{\text{nope}}}$  and  $\mathbf{v}_{t,i}^C \in \mathbb{R}^{d_{\text{nope}}}$ , respectively. The position-independent query for the  $i$ -th head is represented as  $\mathbf{q}_{t,i}^C \in \mathbb{R}^{d_{\text{nope}}}$ . The computations for the attention mechanism proceed as follows:

$$\mathbf{c}_t^{KV} = W_{\text{DKV}} \mathbf{h}_t, \quad (15)$$

$$\mathbf{k}_{t,i}^C = W_{\text{UK},i} \mathbf{c}_t^{KV}, \quad (16)$$

$$\mathbf{k}_t^R = \text{RoPE}(W_{\text{KR}} \mathbf{h}_t), \quad (17)$$

$$\mathbf{k}_{t,i} = [\mathbf{k}_{t,i}^C; \mathbf{k}_t^R], \quad (18)$$

$$\mathbf{q}_{t,i}^C = W_{\text{Q},i} \mathbf{h}_t, \quad (19)$$

$$\mathbf{q}_{t,i}^R = \text{RoPE}(W_{\text{QR},i} \mathbf{h}_t), \quad (20)$$

$$\mathbf{q}_{t,i} = [\mathbf{q}_{t,i}^C; \mathbf{q}_{t,i}^R], \quad (21)$$

$$\mathbf{v}_{t,i}^C = W_{\text{UV},i} \mathbf{c}_t^{KV}, \quad (22)$$

where  $W_{\text{DKV}} \in \mathbb{R}^{d_c \times H}$  is the down-projection matrix for key-value compression,  $W_{\text{UK},i} \in \mathbb{R}^{d_{\text{nope}} \times d_c}$  and  $W_{\text{UV},i} \in \mathbb{R}^{d_{\text{nope}} \times d_c}$  are the up-projection matrices for decompressed key and value for the  $i$ -th head,  $W_{\text{KR}} \in \mathbb{R}^{d_{\text{nope}} \times H}$  generates the shared positional key component via RoPE [40], and  $W_{\text{Q},i} \in \mathbb{R}^{d_{\text{nope}} \times H}$  and  $W_{\text{QR},i} \in \mathbb{R}^{d_{\text{nope}} \times H}$  generate the position-independent and RoPE-enhanced query components for the  $i$ -th head.

The attention outputs  $\{\mathbf{o}_{t,i}\}$  are calculated as follows:

$$\mathbf{o}_{t,i} = \sum_{j=1}^t \text{Softmax}_j \left( \frac{\mathbf{q}_{t,i}^\top \mathbf{k}_{j,i}}{\sqrt{d_h}} \right) \mathbf{v}_{j,i}^C, \quad (23)$$

where  $d_h = d_{\text{nope}} + d_{\text{rope}}$  represents the total head dimension. The final output is obtained by combining the attention results from all heads through a linear projection:

$$\mathbf{u}_t = W_{\text{O}} [\mathbf{o}_{t,1}; \mathbf{o}_{t,2}; \dots; \mathbf{o}_{t,n_h}], \quad (24)$$

where  $W_{\text{O}} \in \mathbb{R}^{H \times d_{\text{nope}} n_h}$  is the output projection matrix and  $n_h$  is the number of attention heads.

### B.2.2 Prefill

Let the input sequence length be  $N$ . The computational complexity for projecting the context vector  $\mathbf{c}_t^{KV}$  is  $\mathcal{O}(d_c NH)$ . Subsequent projections for content-based keys  $\mathbf{k}_{t,i}^C$  and values  $\mathbf{v}_{t,i}^C$  require  $\mathcal{O}(2d_c d_{\text{nope}} N)$  operations, while the query projection  $\mathbf{q}_{t,i}^C$  incurs  $\mathcal{O}(d_{\text{nope}} NH)$ . For rotary position embeddings (RoPE), the projections for  $\mathbf{k}_t^R$  and  $\mathbf{q}_{t,i}^R$  each demand  $\mathcal{O}(d_{\text{rope}} NH)$ . The output projection further adds  $\mathcal{O}(NH^2)$ .

The total computational linear projection cost for generating keys  $\{\mathbf{k}_{t,i}\}$ , queries  $\{\mathbf{q}_{t,i}\}$ , values  $\{\mathbf{v}_{t,i}\}$  and outputs  $\mathbf{o}_t$  combines these components:

$$\mathcal{O}((d_c + d_{\text{rope}})NH + n_h(d_{\text{nope}} + d_{\text{rope}})NH + 2n_h d_c d_{\text{nope}} N + NH^2).$$

The attention mechanism's computational complexity arises from pairwise interactions between sequence elements, resulting in a quadratic scaling with sequence length  $N$ . Computing attention scores  $QK^T$  has a complexity of  $\mathcal{O}(n_h(d_{\text{rope}} + d_{\text{nope}})N^2)$ . Generating the attention output by values  $V$  adds  $\mathcal{O}(n_h d_{\text{nope}} N^2)$ . The total complexity is thus  $\mathcal{O}(n_h(d_{\text{rope}} + 2d_{\text{nope}})N^2)$ .

Aggregating all terms, the overall computational complexity becomes:

$$\begin{aligned} \text{Prefill}_{\text{mla}} = & \\ \mathcal{O}((d_c + d_{\text{rope}})NH + n_h(d_{\text{nope}} + d_{\text{rope}})NH + 2n_h d_c d_{\text{nope}} N + NH^2 + n_h(d_{\text{rope}} + 2d_{\text{nope}})N^2) & \end{aligned} \quad (25)$$

### B.2.3 Decode

Consider an input sequence of length  $N - 1$ . The computational complexity to generate the  $N$ -th token's joint compression state  $\mathbf{c}_N^{KV}$  is  $\mathcal{O}(d_c H)$ . Subsequent projections for the rotary position embedding (RoPE)-based key  $\mathbf{k}_N^R$  and query  $\mathbf{q}_{N,i}^R$  each require  $\mathcal{O}(d_{\text{rope}} H)$ , while the content-based query  $\mathbf{q}_{N,i}^C$  incurs  $\mathcal{O}(d_{\text{nope}} H)$ . For historical tokens  $t = 1, \dots, N$ , the projections of content-based keys  $\{\mathbf{k}_{t,i}^C\}$  and values  $\{\mathbf{v}_{t,i}^C\}$  scale as  $\mathcal{O}(2d_c d_{\text{nope}} N)$ , while the output projection requires  $\mathcal{O}(H^2)$ . The total computational linear projection cost:

$$\mathcal{O}((d_c + d_{\text{rope}})H + n_h(d_{\text{nope}} + d_{\text{rope}})H + 2n_h d_c d_{\text{nope}} N + H^2).$$

The attention mechanism's computational complexity arises from pairwise interactions between sequence elements. Computing attention scores  $QK^T$  has a complexity of  $\mathcal{O}(n_h(d_{\text{rope}} + d_{\text{nope}})N)$ . Generating the attention output by values  $V$  adds  $\mathcal{O}(n_h d_{\text{nope}} N)$ . The total complexity is thus  $\mathcal{O}(n_h(d_{\text{rope}} + 2d_{\text{nope}})N)$ . Combining these components, the total computational cost is:

$$\text{Generate}_{\text{mla}} = \mathcal{O}((d_c + d_{\text{rope}})H + n_h(d_{\text{nope}} + d_{\text{rope}})H + 2n_h d_c d_{\text{nope}} N + H^2 + (n_h(d_{\text{rope}} + 2d_{\text{nope}})N).$$

Caching mechanisms store the joint compression states  $\{\mathbf{c}_t^{KV}\}_{t=1, \dots, N-1}$  and RoPE keys  $\{\mathbf{k}_t^R\}_{t=1, \dots, N-1}$ , with memory footprint:

$$\text{Cache}_{\text{mla}} = (d_{\text{rope}} + d_c)N.$$

## B.3 GQA

### B.3.1 Definition

Let  $\mathbf{h}_t \in \mathbb{R}^H$  represent the input hidden state for the  $t$ -th token in the attention mechanism. The grouped key and value for the  $j$ -th kv head are denoted by  $\mathbf{k}_{t,j} \in \mathbb{R}^{d_h}$  and  $\mathbf{v}_{t,j} \in \mathbb{R}^{d_h}$ , respectively. The position-independent query for the  $i$ -th head is represented as  $\mathbf{q}_{t,i} \in \mathbb{R}^{d_h}$ . The computations for the attention mechanism proceed as follows:

$$\mathbf{k}_{t,j} = \text{RoPE}(W_{K,j} \mathbf{h}_t), \quad (26)$$

$$\mathbf{q}_{t,i} = \text{RoPE}(W_{Q,i} \mathbf{h}_t), \quad (27)$$

$$\mathbf{v}_{t,j}^C = W_{V,j} \mathbf{h}_t, \quad (28)$$

where  $W_{K,j} \in \mathbb{R}^{d_h \times H}$  and  $W_{V,j} \in \mathbb{R}^{d_h \times H}$  are the up-projection matrices for grouped key and value for the  $j$ -th kv head, and  $W_{Q,i} \in \mathbb{R}^{d_h \times H}$  for the  $i$ -th head, respectively.

The attention outputs  $\{\mathbf{o}_{t,i}\}$  are calculated as follows:

$$\mathbf{o}_{t,i} = \sum_{k=1}^t \text{Softmax}_k \left( \frac{\mathbf{q}_{t,i}^\top \mathbf{k}_{k,i \bmod n_k}}{\sqrt{d_h}} \right) \mathbf{v}_{k,i \bmod n_k}, \quad (29)$$

The final output is obtained by combining the attention results from all heads through a linear projection:

$$\mathbf{u}_t = W_O [\mathbf{o}_{t,1}; \mathbf{o}_{t,2}; \dots; \mathbf{o}_{t,n_h}], \quad (30)$$

where  $W_O \in \mathbb{R}^{H \times d_{\text{nope}} n_h}$  is the output projection matrix and  $n_h$  is the number of attention heads.

### B.3.2 Prefill

For an input sequence of length  $N$ , the computational complexity begins with the projection operations for keys  $\mathbf{k}_{t,j}$  and values  $\mathbf{v}_{t,j}$ , each requiring  $\mathcal{O}(2d_h N H)$  operations. The query projection  $\mathbf{q}_{t,i}$  further contributes  $\mathcal{O}(d_h N H)$ . The output projection requires  $\mathcal{O}(H^2)$ .

Respectively. Aggregating these components, the total linear projection cost becomes:

$$\mathcal{O}(2NH^2 + 2n_k d_h NH).$$

The attention mechanism's computational complexity arises from pairwise interactions between sequence elements, resulting in a quadratic scaling with sequence length  $N$ . Computing attention scores  $QK^T$  has a complexity of  $\mathcal{O}(n_h d_h N^2)$ . Generating the attention output by values  $V$  adds  $\mathcal{O}(n_h d_h N^2)$ . The total complexity is thus  $\mathcal{O}(2n_h d_h N^2)$ .

Combining all terms, the total computational complexity for the prefill phase is:

$$\text{Prefill}_{gqa} = \mathcal{O}(2NH^2 + 2n_k d_h NH + 2n_h d_h N^2).$$

### B.3.3 Decode

For an input sequence of length  $N - 1$ , the decoder phase computes the  $N$ -th token's representations through successive transformations. Key and value projections  $\mathbf{k}_{N,j}$  and  $\mathbf{v}_{N,j}$  require  $\mathcal{O}(2d_h H)$  operations, while the query projection  $\mathbf{q}_{N,i}$  incurs  $\mathcal{O}(d_h H)$ . The total computational linear projection cost:

$$\mathcal{O}(2H^2 + 2n_k d_h H).$$

The attention mechanism, operating over cached historical states, scales as  $\mathcal{O}(2n_h d_h N)$ , reflecting linear dependence on sequence length  $N$ . Aggregating all components, the total computational cost is:

$$\text{Generate}_{gqa} = \mathcal{O}(2H^2 + 2n_k d_h H + 2n_h d_h N).$$

Caching historical keys  $\{\mathbf{k}_{t,j}\}$  and values  $\{\mathbf{v}_{t,j}\}$  for  $t = 1, \dots, N - 1$  demands memory:

$$\text{Cache}_{gqa} = 2n_k d_h N,$$

## C Efficiency Analysis

### C.1 Additional Empirical Benchmarks with LLM-Viewer

To comprehensively evaluate the robustness of GTA-1B’s performance across diverse hardware platforms, we conducted extensive benchmarks using the `LLM-Viewer` framework, consistent with our main evaluation methodology. These experiments were performed on various NVIDIA GPUs, including NVIDIA A100 40GB, NVIDIA A100 80GB, NVIDIA H100 80GB, NVIDIA H100 PCIe 80GB. As presented in [Figure 13](#), [Figure 12](#), [Figure 14](#), and [Figure 15](#). The results consistently demonstrate GTA-1B’s performance advantages over GQA-1B across all tested configurations.

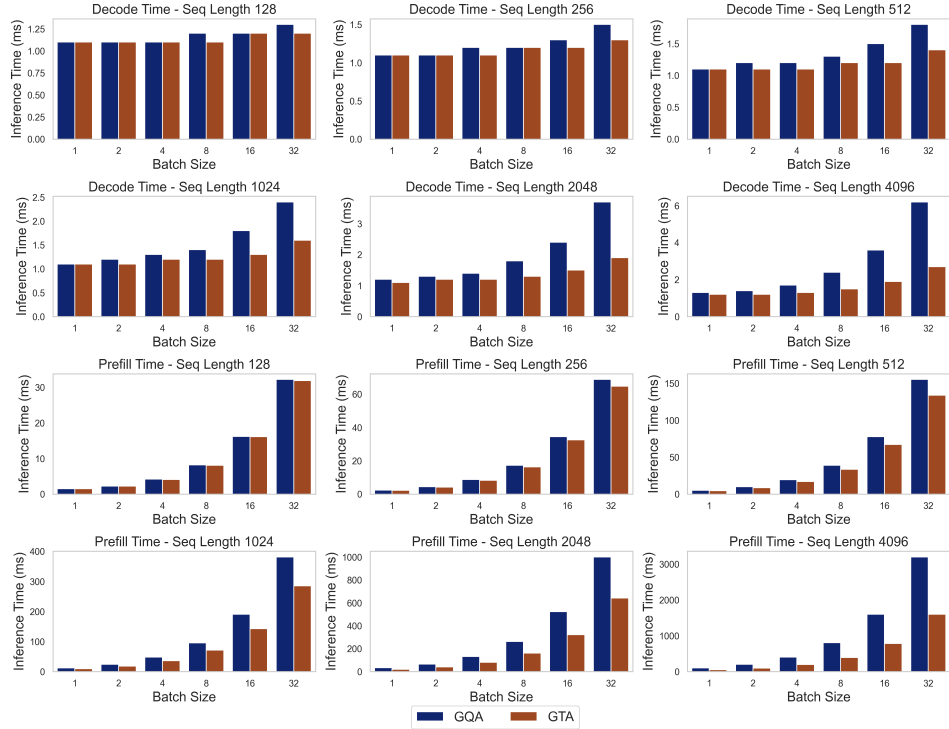


Figure 12: Prefill and decode times for GTA-1B and GQA-1B across configurations on an NVIDIA A100 80GB GPU.

These findings align with our primary results (e.g NVIDIA A100 80GB GPU), further reinforcing GTA-1B’s scalability and adaptability across various hardware platforms. Notably, the I/O-bound decode phase shows significant benefits owing to GTA-1B’s optimized memory access patterns. Collectively, these results provide robust evidence for the practical utility of GTA-1B in diverse real-world deployment scenarios.

### C.2 Additional Practical Inference Deployments

In this appendix, we provide detailed information about our experimental setup and present additional benchmark results for GTA-1B and GQA-1B under half-precision computations.

We conducted comprehensive benchmarks using the `transformers` library (version 4.36.0) to evaluate the practical performance of our models across various hardware platforms. The experimental setup included the following specifications:

- **Hardware:** NVIDIA H100 80GB, NVIDIA A800 80GB, NVIDIA RTX 3060 12GB, Apple M2, and BCM2712
- **Precision:** Both full-precision (FP32, main text) and half-precision (FP16/BF16, this appendix)

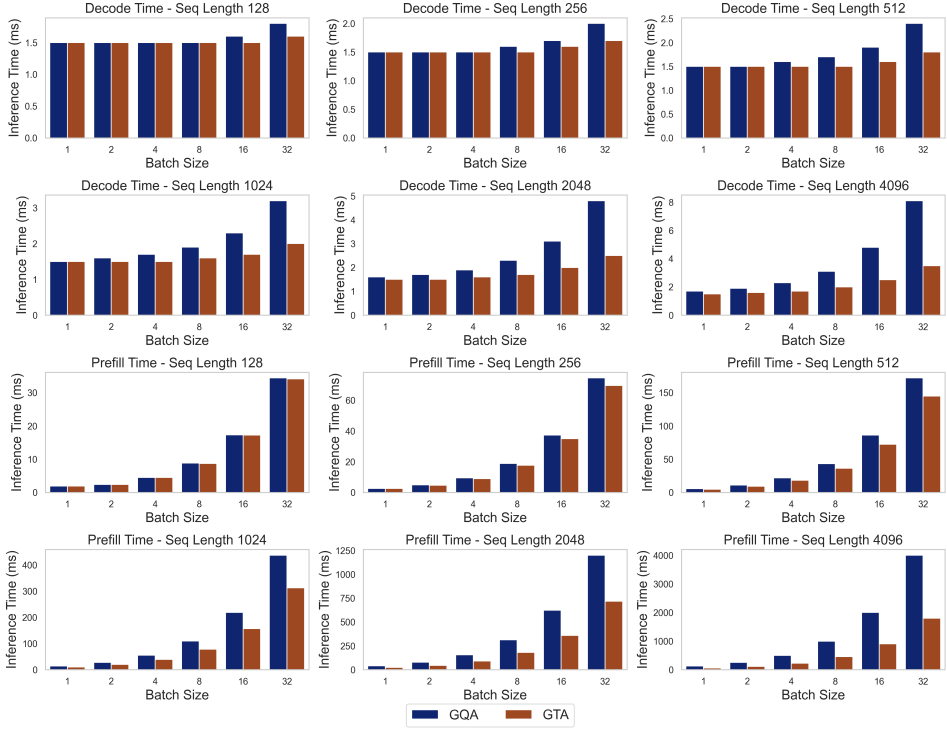


Figure 13: Prefill and decode times for GTA-1B and GQA-1B across configurations on an NVIDIA A100 40GB GPU.

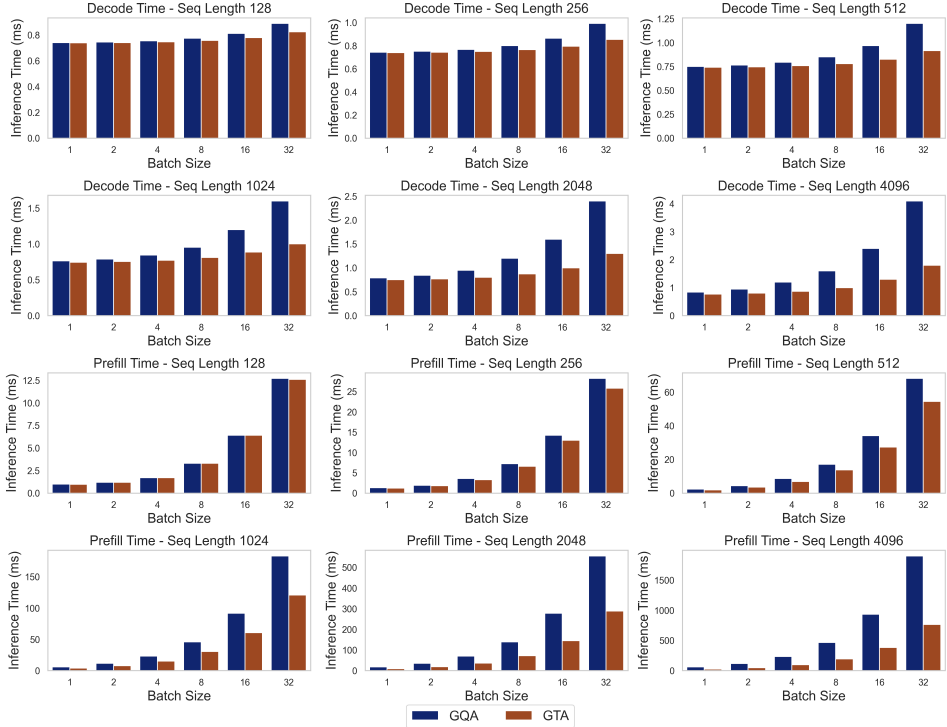


Figure 14: Prefill and decode times for GTA-1B and GQA-1B across configurations on an NVIDIA H100 80GB GPU.

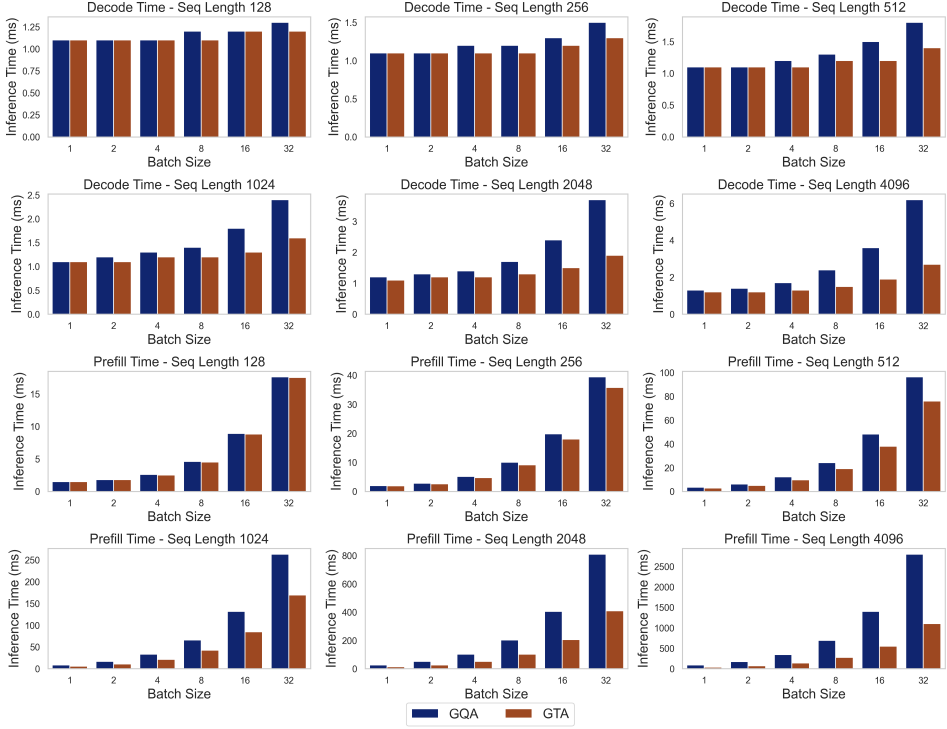


Figure 15: Prefill and decode times for GTA-1B and GQA-1B across configurations on an NVIDIA H100 PCIe 80GB GPU.

- **Input Lengths:** 128, 512, 1024 and 2048 tokens

For KV cache implementation, we used two approaches:

- **Standard benchmarks:** `DynamicCache` (default in transformers)
- **Offload benchmarks:** `OffloadedStaticCache` (allocates fixed memory, pre-caches two layers on GPU)

All results represent the average of three stable runs after a warm-up phase.

While the main text presented full-precision results, here we provide complementary half-precision benchmarks that demonstrate similar performance patterns but with overall improved efficiency across all hardware platforms.

Figure 16 shows half-precision performance without cache offload. Similar to full-precision results in the main text, GTA-1B (blue solid line) consistently outperforms GQA-1B (orange dashed line). The performance advantage becomes more pronounced at longer sequence lengths, with GTA-1B demonstrating improved efficiency in both prefill and decode phases.

Figure 17 presents the half-precision results with cache offload enabled. GTA-1B's efficiency advantage is further enhanced in this memory-constrained scenario, especially on the NVIDIA A800 80GB at longer sequence lengths. This confirms that GTA-1B's optimized memory access patterns are particularly effective in I/O-bound scenarios, consistent with the full-precision findings reported in the main text. These half-precision benchmarks demonstrate that GTA-1B maintains its performance advantages over GQA-1B across different precision settings, validating the architecture's practical efficiency for real-world deployment scenarios.

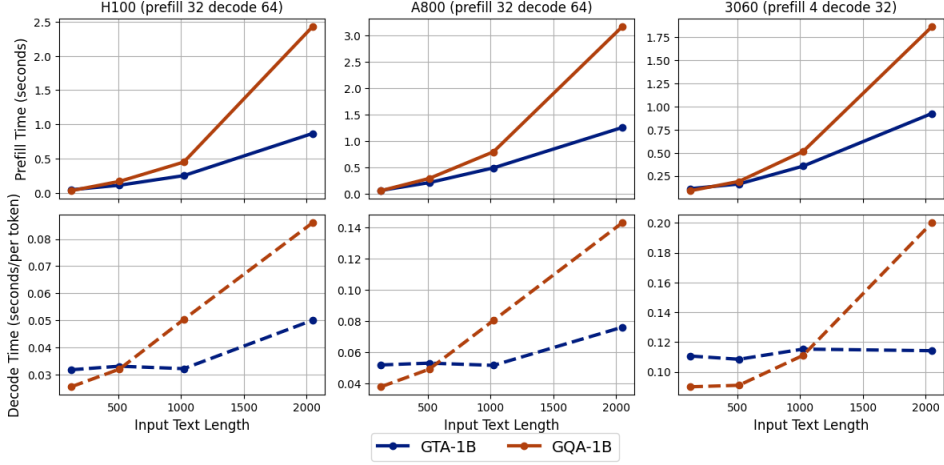


Figure 16: Half-precision prefill and decode times for GTA-1B and GQA-1B across configurations on NVIDIA H100, NVIDIA A800, RTX 3060.

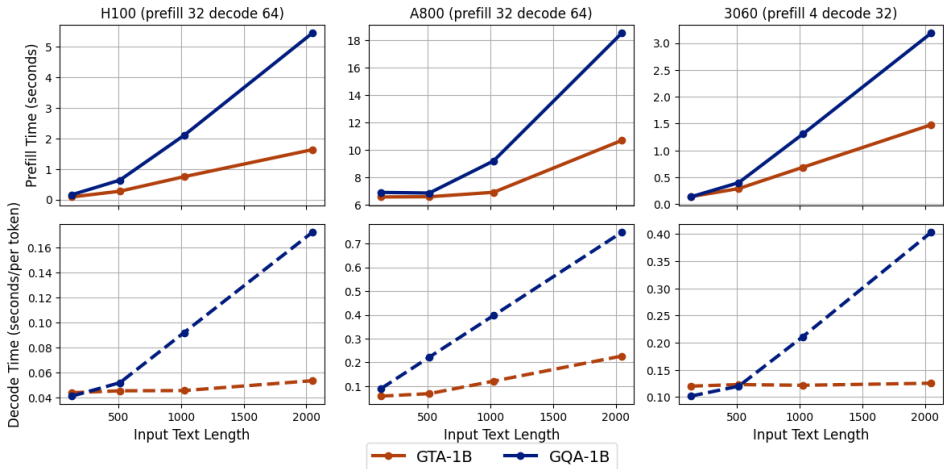


Figure 17: Half-precision prefill and decode performance of GTA-1B and GQA-1B models with cache offload, evaluated on diverse hardware platforms across various test configurations.